Chiral cilia orientation in the left-right organizer

Rita R. Ferreira[1,2,3,4], Guillaume Pakula[5], Andrej Vilfan[6], Willy Supatto[5] and Julien Vermot[1,2,3,4]

[1]Institut de Génétique et de Biologie Moléculaire et Cellulaire, Illkirch, France
[2]Centre National de la Recherche Scientifique, UMR7104, Illkirch, France
[3]Institut National de la Santé et de la Recherche Médicale, U964, Illkirch, France
[4]Université de Strasbourg, Illkirch, France
[5]Laboratory for Optics and Biosciences, Ecole Polytechnique, Centre National de la Recherche Scientifique (UMR7645), Institut National de la Santé et de la Recherche Médicale (U1182) and Paris Saclay University, Palaiseau, France
[6]J. Stefan Institute, Ljubljana, Slovenia

Abstract

Chirality is a property of asymmetry between an object and its mirror image. Most biomolecules and cells are intrinsically chiral. Whether cellular chirality can be transferred to asymmetry at the tissue scale remains an unresolved issue. This question is particularly relevant in the left-right organizer (LRO), where cilia motility and chiral flow are thought to be the main drivers of left-right axis symmetry breaking. Here, we built a quantitative approach based on live imaging to set apart the contributions of various pathways to the spatial orientation of cilia in the LRO. We found that cilia populating the zebrafish LRO display an asymmetric orientation between the right and left side of the LRO. We report this asymmetry does not depend on the left-right signalling pathway demonstrating cilia orientation is chiral. Furthermore, we show the establishment of the chirality is dynamic and depends on planar cell polarity. Together, this work identifies a novel type of asymmetry in the LRO, where the chirality is defined by spatial cilia orientation, and sheds light on the complexity of chirality genesis in developing tissues.

A chiral object cannot be superimposed on its mirror image. Most biological molecules are chiral. Yet, how macroscopic chiral asymmetries arise in physics and biology is still debated (Morrow et al., 2017; Wagnière, 2007). In living systems, a number of independent mechanisms of chirality establishment have been identified, from subcellular to tissular scale (Blum et al., 2014; Coutelis et al., 2014; Dasgupta and Amack, 2016; Gomez-Lopez et al., 2014; Hamada and Tam, 2014; Levin, 2005; Naganathan et al., 2014; Noel et al., 2013; Tee et al., 2015). The most studied system is certainly the mechanism that sets asymmetric gene expression around the left-right organizers (LRO) of vertebrates. Generally, asymmetrical signals are generated in LROs as a response to a directional flow driven by motile cilia (Shinohara and Hamada, 2017). In the LRO, the orientation of cilia rotation is chiral and invariable amongst vertebrates (Okada et al., 2005). These properties are key for controlling the chiral direction of the flow (Hilfinger and Julicher, 2008; Shinohara and Hamada, 2017).

In zebrafish, the LRO is called the Kupffer's vesicle (KV) (Figure 1A). Before any sign of asymmetric cell response, the KV consists of a sphere containing monociliated cells where a directional flow progressively emerges as a result of stereotyped cilia spatial orientation (Ferreira et al., 2017). Over the course of hours, the cilia-generated flow triggers an asymmetric calcium response on the left side of the cavity (Francescatto et al., 2010; Sarmah et al., 2005; Yuan et al., 2015), and, consequently, a left-biased asymmetric pattern of gene expression (Essner et al., 2005; Kramer-Zucker et al., 2005). Coordinating appropriate cilia spatial orientation with directional flow generation is thus critical for the subsequent asymmetric response and proper LR patterning (Hashimoto and Hamada, 2010). Current studies have posited that flow patterns arise first in the LRO and then dictate the symmetry-breaking event (Blum et al., 2014; Shinohara and Hamada, 2017). This has led to the inference that symmetry breaking initiation depends on the establishment of symmetrical LRO where cilia orientation is tightly controlled by the Planar Cell Polarity (PCP) pathway (Hashimoto and Hamada, 2010; Marshall and Kintner, 2008; Song et al., 2010). In this model, the direction of cilia rotation leading to the directional flow is the only known chiral element in the LRO. However, a number of studies have suggested that subcellular chirality associated with cytoskeletal asymmetric order could also participate in setting the LR axis, in particular in asymmetric animals where no LRO have been identified (Davison et al., 2016; Hozumi et al., 2006; Kuroda et al., 2009; Sato et al., 2015; Shibazaki et al., 2004; Speder et al., 2006). This raises the intriguing possibility that the LRO could use subcellular chiral information for symmetry breaking. In the absence of tools for visualizing potential chirality in the LRO, however, it is difficult to establish if cell chirality could participate in the process of symmetry breaking. To meet this challenge, we developed a quantitative analysis based on live imaging allowing the accurate extraction of information about the LRO chirality and the identification of the factors controlling it.

Tissue chirality can result from asymmetric cell shape and asymmetric organelle distribution at the cell scale (Wan et al., 2011; Xu et al., 2007). We reasoned that as an asymmetry generator, the LRO itself constitutes a candidate for being a chiral organ. We hypothesized that as an extension of the cytoskeleton, cilia

orientation could be a good read-out of cellular chirality. We made use of the almost perfect elipsoidicity of the KV to assess the symmetry of cilia orientation by focusing on the two angles defining cilia orientation in 3D, *Theta* (θ) and *Phi* (φ) (Figure 1B): θ (tilt) is the angle of the cilium with respect to the KV surface normal (0° for a cilium orthogonal to the KV surface and 90° for parallel); φ is the orientation of the cilium projected on the KV surface (0° for a cilium pointing in a meridional direction towards the dorsal pole). Thus, the meridional tilt of cilia reported in wild-type (WT) KV corresponds to $\theta > 0°$ and φ close to 0° (Ferreira et al., 2017). We performed live-imaging using the zebrafish *act2b:Mmu.Arl13bGFP* transgenic line where cilia are fluorescently labelled (Borovina et al., 2010). Next, we extracted the θ_{avg} and φ_{avg} angles of the average cilia orientation vector on both hemispheres of the KV between the 9 and 14 somites stage (SS), when the chiral flow is fully established. To quantify cilia orientation between the left and right sides, we calculated separately for each side the average cilium direction in local coordinates (Figure 1B). In analogy to an individual cilium, the angles φ_{avg} and θ_{avg} describe the direction of the average orientation vector on each side. In case of a mirror-symmetric KV, θ_{avg} of the average cilium is equal on the left and on the right sides and the φ_{avg} angles are mirror-imaged: $\theta_{avg_left} = \theta_{avg_right}$, and $\varphi_{avg_left} = -\varphi_{avg_right} = \varphi_{avg_right_mirror}$. To quantitatively assess the significance of asymmetries in the KV, we designed a permutation test based on the definition of chirality (see Methods) and calculated p-values estimating the likelihood that an *a priori* symmetric KV will show an equal or larger difference $|\varphi_{avg_left} - \varphi_{avg_right\ mirror}|$ due to variability.

We extracted and averaged the results obtained from 14 WT vesicles with a total of 741 cilia, and estimated the θ_{avg} and φ_{avg} angles of the average cilium in 3D. There was a difference between the measured φ angle on the left and the right sides of the KV (Figure 1C). While right-sided cilia are almost perfectly oriented along the meridional direction ($\varphi_{avg_right} = +1°$, Figure 1D-E), cilia on the left hemisphere exhibit a strong tilt following the direction of the flow ($\varphi_{avg_left} = +27°$, Figure 1D-E). On average, it defines a dextral orientation over the whole vesicle (Sup. Figure 2A). The permutation test confirmed the significance ($p<0.001$) of the observed asymmetry in cilia orientations between the left and right side of the KV ($\varphi_{avg_left} \neq -\varphi_{avg_right}$) (Methods and Table 1). No difference in tilt angles was observed between the left and right hemispheres ($\theta_{avg_left} = \theta_{avg_right}$; Sup. Figure 1). Together, these results show that cilia orientation is asymmetric in the KV and follows a dextral chirality.

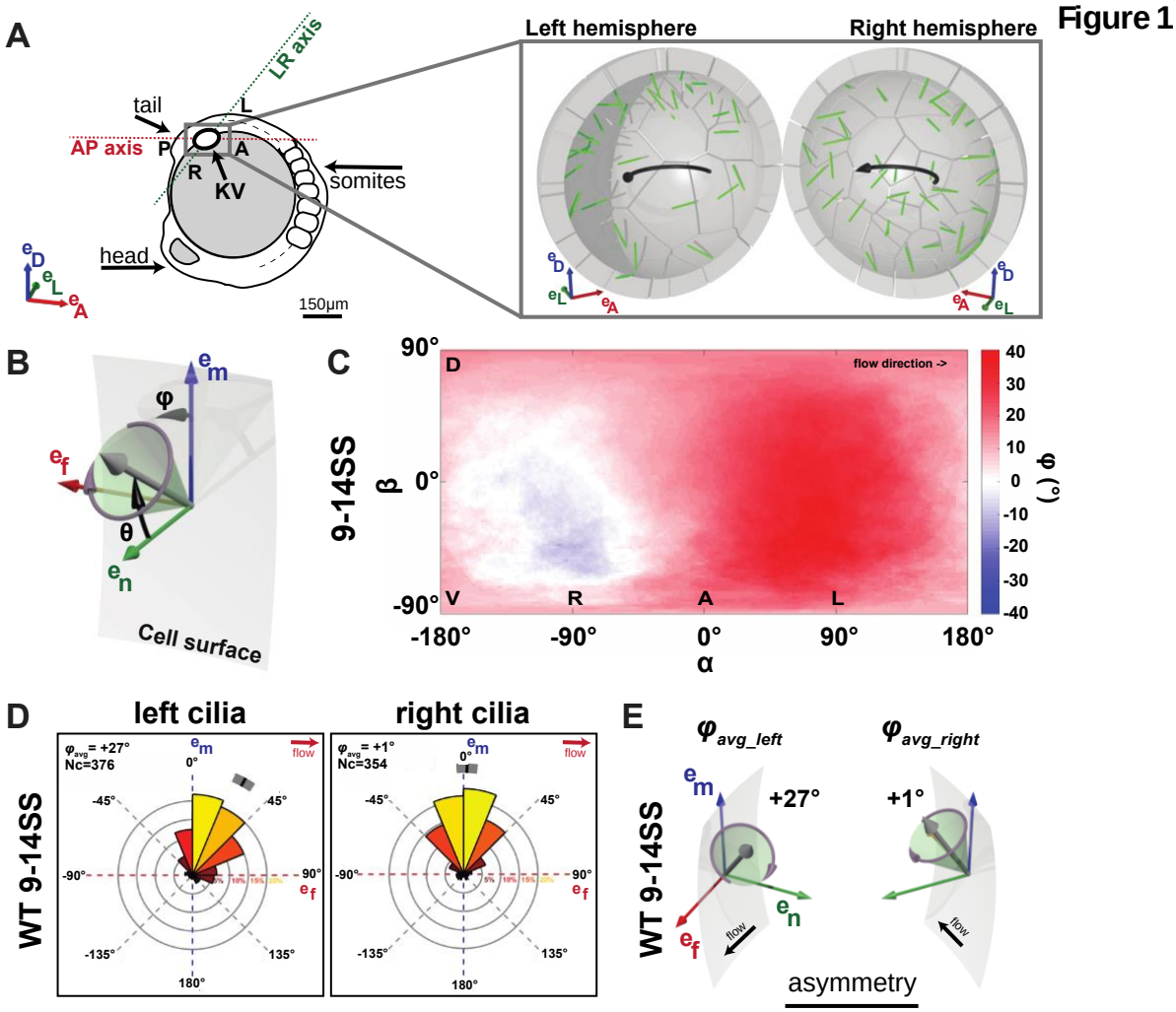

Figure 1: The zebrafish left-right organizer is asymmetric. (A) Schematics of the side-view position of the KV in the zebrafish embryo (left panel) highlighting the KV localization (grey box). The zoom-up box (right panel) shows the schematic transverse section of the KV, depicting the cilia (in green) and the directional flow (black arrows). The embryonic body plan axes are marked as AP (anterior-posterior) and LR (left-right). The body plan reference frame is defined by basis vectors e_D (dorsal), e_L (left), e_A (anterior). **(B)** Cilia orientations are represented by two angles: θ (tilt angle from the surface normal e_n) and φ (angle between the surface projection of the ciliary vector and the meridional direction e_m). Cell surface is represented in grey, e_m direction in blue, e_f direction in red and the normal e_n in green. **(C-D)** Distributions of φ at 9-14SS for KV cilia in a 2D flat map (C) or rosette plots (D) obtained from 14 wild-type vesicles with a total of 741 cilia. **(C)** Average φ values displayed in a 2D flat map showing φ on the left (0° ≤ α ≥ 90° and -90° ≤ β ≥ 90°) is higher (red) than φ on the right (-90° ≤ α ≥ 0° and -90° ≤ β ≥ 90°). **(D)** Rosette plots showing the φ angle distribution for the left and right-sided cilia, and the 95% confidence interval (grey stripe) for the population mean (black tick). In each rosette, 0° indicates the meridional direction (e_m) and 90° the flow direction (e_f). We count cilia exhibiting φ angles between [-45°; +45°] as having a meridional tilt (Ferreira et al., 2017). **(E)** Schematics showing the φ_{avg} of the 3D resultant vector on the left and right sides of the KV at 9-14SS. Nc = number of cilia

To gain a better sense of when the chirality of cilia orientation begins, we analyzed cilia orientation in KV of different stages. We quantified the φ angle distributions of cilia from both hemispheres of WT embryos at 3SS (early-stage), when the first signs of LR asymmetry have been reported (Yuan et al., 2015), and at 8SS (mid-stage). At 3SS, two populations of cilia exist in the KV, motile and immotile. Neither the motile (φ_{avg_left} = +14° and φ_{avg_right} = -21°; Figure 2A-B), nor the immotile cilia population (φ_{avg_left} = +32° and φ_{avg_right} = -8°; Sup. Figure 2B) exhibit a significant difference between the left and right sides of the KV. Permutation test reveals no sign of asymmetry in cilia orientation ($\varphi_{avg_left} \approx - \varphi_{avg_right}$, Table 1), resulting in a φ_{avg} close to 0° at 3SS (Figure 3A). Interestingly, at 8SS the side-biased orientation (φ_{avg_left} = +19° and φ_{avg_right} = +4°; Figure 2A-B) becomes significant enough to reveal an overall asymmetry of the KV (Figure 3A and Table 1). When considering θ angle distributions at 3 and 8SS, we did not find any asymmetry between the left and right-side of the KV, demonstrating that the cilia tilt remains symmetrical over time (Sup. Figure 1). Together, these results demonstrate that cilia orientation in the LRO does not exhibit any asymmetry at early stages and becomes progressively asymmetric during the course of KV development and LR patterning.

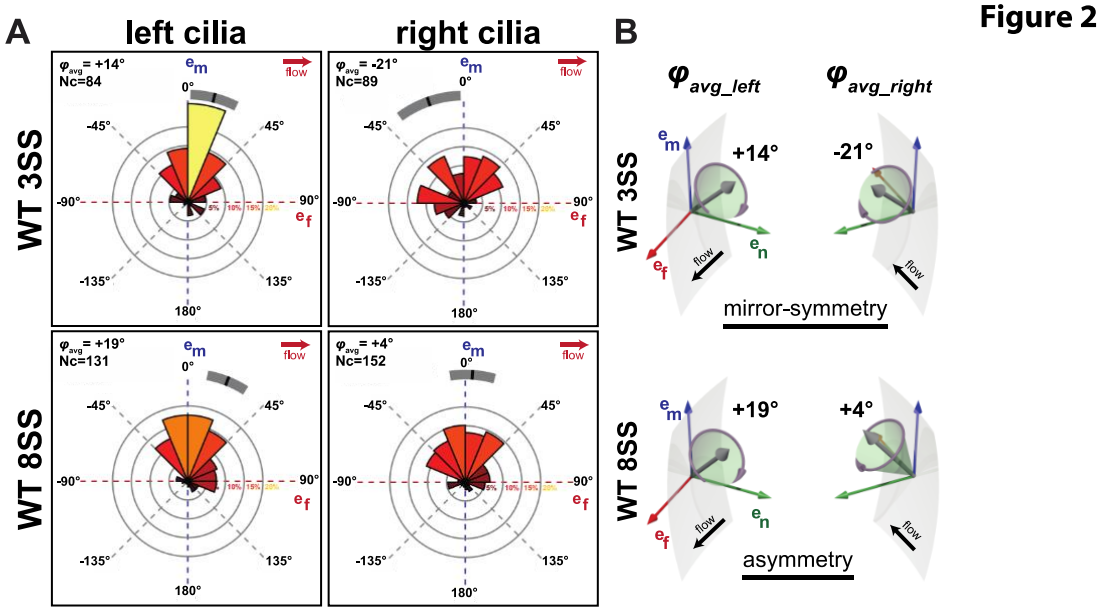

Figure 2: Asymmetric cilia orientation arises over time. (A) Rosette plots showing the φ angle distribution values for the left- (left panel) and right-sided (right panel) cilia, with their mean (black tick) and associated 95% confidence interval (grey stripe), for WT 3SS (upper panel) and WT 8SS (lower panel). In each rosette, 0° indicates the meridional direction (e_m) and 90° the flow direction (e_f). We count cilia exhibiting φ angles between [-45°; +45°] as having a meridional tilt (Ferreira et al., 2017). **(B)** Schematics showing the φ_{avg} of the 3D resultant vector on the left and right sides of the KV at 3SS (upper panel) and 8SS (lower panel). Nc = number of cilia

Considering the function of the KV is to generate an asymmetrical signal, we investigated whether the observed asymmetry of the KV itself is modulated by the LR signalling pathway. According to current models of symmetry breaking, the asymmetric expression of genes around the LRO is under the control of *pkd2* that acts as a flow sensor and leads to the left-sided expression of *spaw*, a nodal-related gene involved in the establishment of the left-right asymmetry (Schottenfeld et al., 2007; Yuan et al., 2015). To test the impact of flow sensing and asymmetric gene expression downstream of flow on asymmetric cilia orientation, we used *cup*^{tc241} (Schottenfeld et al., 2007) and *spaw*^{s457} (Kalogirou et al., 2014) mutants where *pkd2* and *spaw* are not functional, respectively. As expected, both *cup*$^{-/-}$ and *spaw*$^{-/-}$ embryos have laterality defects (Sup. Figure 3B-C and Table 2). By analyzing the KV cilia orientation, we found a normal meridional orientation of cilia (Sup. Figure 2C, $\varphi_{avg} \neq 0°$ in Figure 3A) and permutation test concluded on the existence of an overall asymmetry in the KV ($\varphi_{avg_left} \neq - \varphi_{avg_right}$) in both *cup*$^{-/-}$ and *spaw*$^{-/-}$ KV cilia at 8SS. Together these results indicate that asymmetric cilia orientation is not dependent upon the LR signalling cascade in the LRO.

Actomyosin contractility is a well-known modulator of tissue chirality *in vitro* (Wan et al., 2011), and *in vivo* during early development of asymmetry in Xenopus embryos (Qiu et al., 2005), and cardiac looping in vertebrate embryos (Noel et al., 2013; Taber, 2006). In addition, actomyosin contractility is required for basal body migration to the apical surface of cells to form cilia (Hong et al., 2015; Pitaval et al., 2010), and it has also been shown to be important to control cell-cell tension during the KV morphogenesis (Wang et al., 2012) and LR determination (Gros et al., 2009; Tabin and Vogan, 2003; Wang et al., 2012). We thus assessed the impact of the actomyosin contractility on asymmetric cilia orientation. To do so, we used blebbistatin and the *rock2b*-morpholino (*rock2b*-MO), to block myosin-II activation (Wang et al., 2011). Both blebbistatin-treated and *rock2b*-MO embryos present laterality defects (Sup. Figure 3B-C and Table 2) as previously described (Wang et al., 2011; Wang et al., 2012). Cilia orientation analysis showed the *rock2b*-Myosin-II pathway does not interfere with the meridional tilt of KV cilia (Sup. Figure 2C). Permutation test concluded the KV at 8SS is overall asymmetric ($\varphi_{avg_left} \neq - \varphi_{avg_right}$) for both blebbistatin and *rock2b*-MO ($\varphi_{avg} \neq 0°$ in Figure 3A with corresponding p values; Table 1). Overall these results indicate that asymmetric cilia orientation is not under the control of the *rock2b*-Myosin-II pathway.

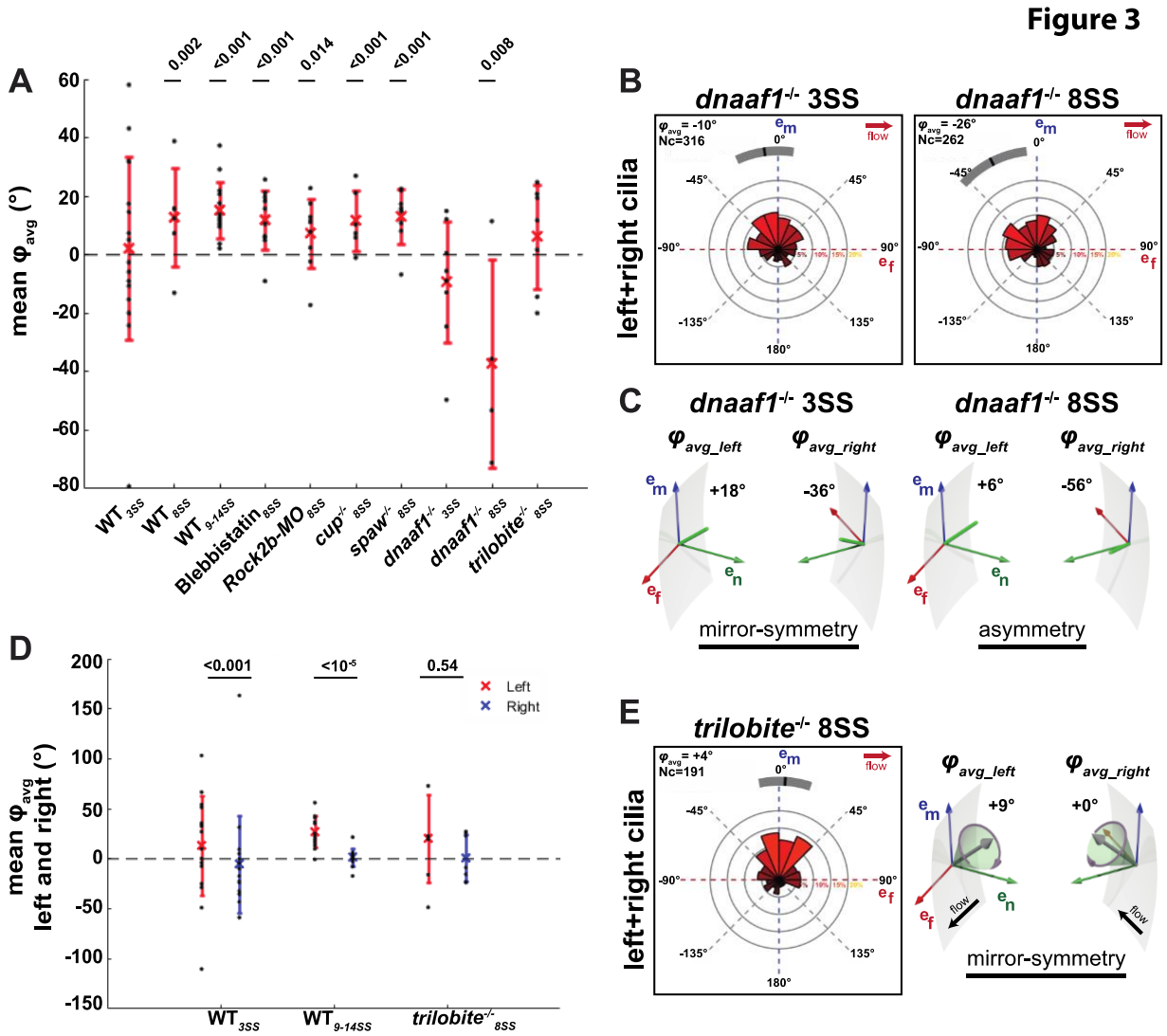

Figure 3: DNAAF1 and PCP are important for asymmetric cilia orientation. (A) Dot plot displaying the mean values of φ_{avg} versus condition. Each black dot represents the mean values for one individual KV, the cross displays the average value for all KVs of the respective condition and the line between the standard deviation. The mean values of φ_{avg} are always greater than zero, except for *dnaaf1*$^{-/-}$ which are below zero, revealing that its orientation with respect to the meridional direction is reversed. Also, WT_{3SS} and *dnaaf1*$^{-/-}{}_{3SS}$ have φ_{avg} mean values close to zero, demonstrating a LR symmetry in the KV. The p-values result from a permutation test under the null hypothesis of a mirror-symmetric KV $\varphi_{avg_left} = -\varphi_{avg_right}$, which is equivalent to $\varphi_{avg} = 0$ (see Methods). **(B)** Rosette plots showing the φ angle distribution values of cilia in both KV hemispheres (left+right cilia), for *dnaaf1*$^{-/-}$ 3SS (upper panel) and *dnaaf1*$^{-/-}$ 8SS (lower panel). Both *dnaaf1*$^{-/-}$ 3SS and *dnaaf1*$^{-/-}$ 8SS cilia are inclined in the opposite direction to the flow (e_f). **(C)** Schematics showing the φ_{avg} of the 3D resultant vector on the left and right sides of the KV for *dnaaf1*$^{-/-}$ 3SS (upper panel) and *dnaaf1*$^{-/-}$ 8SS (lower panel). **(D)** Dot plot displaying the mean values of φ_{avg} on the left (in red) and on the right (in blue) sides of the KV for WT_{3SS}, $WT_{9\text{-}14SS}$ and *trilobite*$^{-/-}{}_{8SS}$. *Trilobite*$^{-/-}{}_{8SS}$ display no difference between the mean φ_{avg} on the left and right sides of the KV. The p-values result from a permutation test under the null hypothesis of $\varphi_{avg_left} = \varphi_{avg_right}$. **(E)** Rosette plot showing the φ angle distribution values of cilia in both KV hemispheres (left+right cilia) for *trilobite*$^{-/-}$ 8SS. In contrast to other conditions studied so far, φ_{avg} of *trilobite*$^{-/-}$ KV cilia is close to zero, reinforcing the fact that the KV is symmetrical at 8SS. **(F)** Schematics showing the φ_{avg} on the left and right sides of the KV for *trilobite*$^{-/-}$ 8SS. Nc = number of cilia.

Ciliary components involved in cilia motility have also been shown to modulate cilia orientation (Jaffe et al., 2016). We thus assessed if cilia motility could be a factor controlling asymmetric cilia orientation. We first analyzed cilia orientation in the WT at 3SS and found that WT immotile cilia have a distinct orientation compared to the motile cilia at the same stage ($\varphi_{avg_WT3SS\ immotile}$ = +13º and $\varphi_{avg_WT3SS\ motile}$ = -3º; Sup. Figure 2A; $p<10^{-4}$), suggesting that motility could be involved in modulating cilia orientation. To confirm that cilia motility is involved, we analyzed the *dnaaf1*$^{-/-}$ *(dynein axonemal assembly factor 1;* old nomenclature: *lrrc50 - leucine-rich repeat-containing protein 50)* mutants. *dnaaf1* encodes for a cilium-specific protein required for the stability of the ciliary architecture and when mutated abrogates its ability to interact with specific targets important for cilia motility (Sullivan-Brown et al., 2008). Importantly, *dnaaf1*$^{-/-}$ cilia have ultrastructural cilia defects and display abnormal dynein arms orientation in beating cilia (Loges et al., 2009). In addition, *dnaaf1* physically interacts with C21orf59/Kurly (Kur), a cytoplasmic protein with some enrichment at the base of cilia and needed for both motility and polarity of beating cilia (Jaffe et al., 2016). We found that all cilia are immotile in the *dnaaf1*$^{-/-}$ KVs (Movie 1) and that LR axis establishment is randomized (Sup. Figure 3B-C and Table 2). We next assessed the existence of a mirror-symmetry at 3 and 8SS in the *dnaaf1*$^{-/-}$ cilia and found that *dnaaf1*$^{-/-}$ cilia orientation does not show any sign of asymmetry at 3SS ($\varphi_{avg_left} \approx - \varphi_{avg_right}$) ($\varphi_{avg} \approx 0°$ in Figure 3A; Figure 3B-C and Table 1), similar to the controls at the same stage (Figure 2 and Sup. Figure 2B). At 8SS, we found that *dnaaf1*$^{-/-}$ cilia orientation is asymmetric ($\varphi_{avg_left} \neq - \varphi_{avg_right}$ in Figure 3B-C and Table 1; $\varphi_{avg} \neq 0°$ in Figure 3A) showing that asymmetric cilia orientation is flow independent. Surprisingly though, we found that *dnaaf1*$^{-/-}$ cilia have a meridional tilt (Figure 3B) but are inclined following a sinistral direction, which is the opposite direction than WT at 8SS ($\varphi_{avg_dnaaf1^{-/-}8SS}$ = -26° (Figure 3B) and $\varphi_{avg_WT8SS\ motile}$ = +11° (Sup. Figure 2A); $p<10^{-5}$. See also Figure 3A with $\varphi_{avg} < 0°$). Thus *dnaaf1* is involved in the control of chiral cilia direction and it may do so independently of the flow.

Finally, since cilia motility and planar cell polarity are interdependent (Jaffe et al., 2016), we directly tested the role of the PCP in KV chirality. It has been shown PCP pathway modulates cilia tilt in the mouse LRO (Hashimoto and Hamada, 2010; Marshall and Kintner, 2008; Song et al., 2010). Generically, PCP proteins are required to establish cell polarity within tissues across a large variety of animal species (Wallingford, 2012). We used the zebrafish *trilobite* mutant line, which locus encodes a Van Gogh/Strabismus homologue - *Van gogh-like 2* (*Vangl2*) -, essential for PCP signalling (Jessen and Solnica-Krezel, 2004). *Vangl2* function is required for the posterior tilt observed in KV cilia, and anomalies in cilia orientation disrupt the cilia-driven flow and LR determination (Borovina et al., 2010) (Sup. Figure 3B-C and Table 2). We studied cilia orientation at 8SS using *trilobite*^{tc240a}*; actb2:Mmu.Arl13b-GFP* (Heisenberg and Nusslein-Volhard, 1997) mutant embryos, and found cilia orientation still follows a meridional tilt (Figure 3E and Sup. Figure 1). Our flow simulations (see Methods and Sup. Figure 3D) predict that flow is significantly weaker in *trilobite*^{tc240a} than in the WT (p=0.024), as expected for a PCP mutant (Borovina et al., 2010). In contrast with other conditions studied so far, permutation test could not detect any asymmetry in the *trilobite*$^{-/-}$ KV cilia at 8SS, meaning $\varphi_{avg_left} = - \varphi_{avg_right}$ (Figure 3E and Table 2). Furthermore, it confirmed that there is no

difference between the two sides of the KV (Figure 3D; p=0.82, Sup. Figure 2), with a $\varphi_{avg} \approx 0°$ (Figure 3A). Altogether, these results indicate the PCP pathway is involved in chiral cilia orientation in the KV.

Discussion

Previous work has focused on identifying signals that trigger the specification of the left embryonic side in response to flow, but the chirality of the LRO remained untested. We took advantage of the zebrafish LRO (KV) as an established model system in which cilia orientation and LR symmetry can be accurately quantified and show that cilia orientation is not symmetrical between the left and right side of the LRO. Our study revealed that cilia orientation progressively changes from mirror-symmetric to asymmetric (Figure 4A) and that this new type of asymmetry emerges independently of the LR symmetry cascade. Considering that several key modulators of symmetry breaking such as Pkd2 or Spaw do not affect cilia orientation, we conclude that the orientation of cilia in the LRO is chiral and that the LRO promotes left-right symmetry breaking and asymmetric cilia orientation through distinct mechanisms. If the asymmetry of cilia orientation is independent of the LR machinery, how can we explain its emergence? One possibility would be that cilia orient according to flow directionality in a similar way that endothelial cells polarize against the flow during blood vessel morphogenesis (Franco et al., 2015; Kwon et al., 2016). We do not favour this hypothesis however because cilia asymmetry is still observed in the *dnaaf1* mutants where flow is absent, and beating cilia are subject to drag forces much stronger than those caused by the directional flow itself (Ferreira et al., 2017). Rather, we propose that the asymmetry could arise from chiral influences generated by the cytoskeletal components that operate at the cellular and subcellular scales (Satir, 2016). In line with this idea is the fact that cells can display chiral behaviours *in vitro* and *in vivo* independently of a LRO (Naganathan et al., 2014; Noel et al., 2013; Speder et al., 2006; Tee et al., 2015). For example, basal body and cilia ultra-structure display obvious signs of chirality (Afzelius, 1976; Marshall, 2012; Pearson, 2014). This suggests two possibilities: either the orientation of the cilia basal bodies is chiral (asymmetric between left and right, Figure 4B), or they are oriented symmetrically and the intrinsic chiral structure of each cilium leads to an overall asymmetric distribution of cilia orientations (Figure 4C). The fact that *dnaaf1*, a cilia specific protein, can reverse cilia orientation from dextral to sinistral seems to argue for the latter. Nevertheless, more work will be needed to establish the molecular basis of cell and cilia chirality in the KV and whether it is conserved in other ciliated LRO.

The demonstration that the asymmetry is actively modulated by the PCP, cilia motility and, potentially, by the internal organization of cilia have important implications for the understanding of chiral information distribution and its control in developing organs. First, it shows that chiral information is dynamic and temporally controlled during the course of LR specification. In that respect, it is interesting to note that cells establish chiral organization as a result of cell migration in vitro (Wan et al., 2011) and that asymmetric cell migration is well described in the chicken LRO (Gros et al., 2009). It is thus possible that the progressive establishment of asymmetric cilia orientation in the LRO reflects an active acquisition of cellular chirality

during the time of LRO function. Second, it indicates that chiral cilia orientation requires the LRO cells to be planar polarized. This raises the intriguing possibility of a more general role of chirality in morphogenetic pattern formation and LR symmetry breaking. Could the chiral cilia orientation participate in symmetry breaking in the LRO? We have previously tested different hypothetical mechanisms of flow detection and shown that a quantitative analysis of physical limits favours chemical sensing (Ferreira et al., 2017). While the basic mechanism of flow generation, as well as flow detection, do not require any prior asymmetry in the KV, we cannot exclude that the ciliary asymmetry participates in the process of symmetry breaking by playing hand-in-hand with the chiral flow to optimize the flow direction or the detection of signalling particles.

More generally, proper orientation of cilia is essential for directed flow generation in ciliated tissues or for swimming in ciliated microorganisms (Goldstein, 2015). An important open question is whether cilia can reorient themselves in the direction of flow (Guirao et al., 2010; Mitchell, 2003) and whether this reorientation is a consequence of hydrodynamic forces, or is it the cell polarity that is affected by the flow. Since some ciliary proteins involved in cilia motility also participate in planar cell polarity (Jaffe et al., 2016), it is possible that the spatial orientation of motile cilia is an intrinsic mechanism which is independent of the flow they generate. In the case of brain cavities, the orientation of cilia beating dynamically follows the circadian rhythm and may be driven by transient changes in cell-cell interactions and in PCP (Faubel et al., 2016). Similarly, ciliated microorganisms can reorient the direction of ciliary beating in the course of an avoidance reaction (Tamm et al., 1975). Our study sheds a different light on these systems as it shows that cilia orientation is related to cell polarity in a complex way that includes an intrinsic sense of chirality. Furthermore, as there is increasing evidence that congenital diseases like idiopathic scoliosis (Grimes et al., 2016), *Kartagener* syndrome, neonatal respiratory distress, hydrocephaly, and male infertility involve cilia motility (Mitchison and Valente, 2017), precise cilia orientation analysis becomes critical to understand the biological principles that govern cilia function and their potential involvement in pathology. In this context, our conclusions and method could be relevant in the studies of a variety of developing organs.

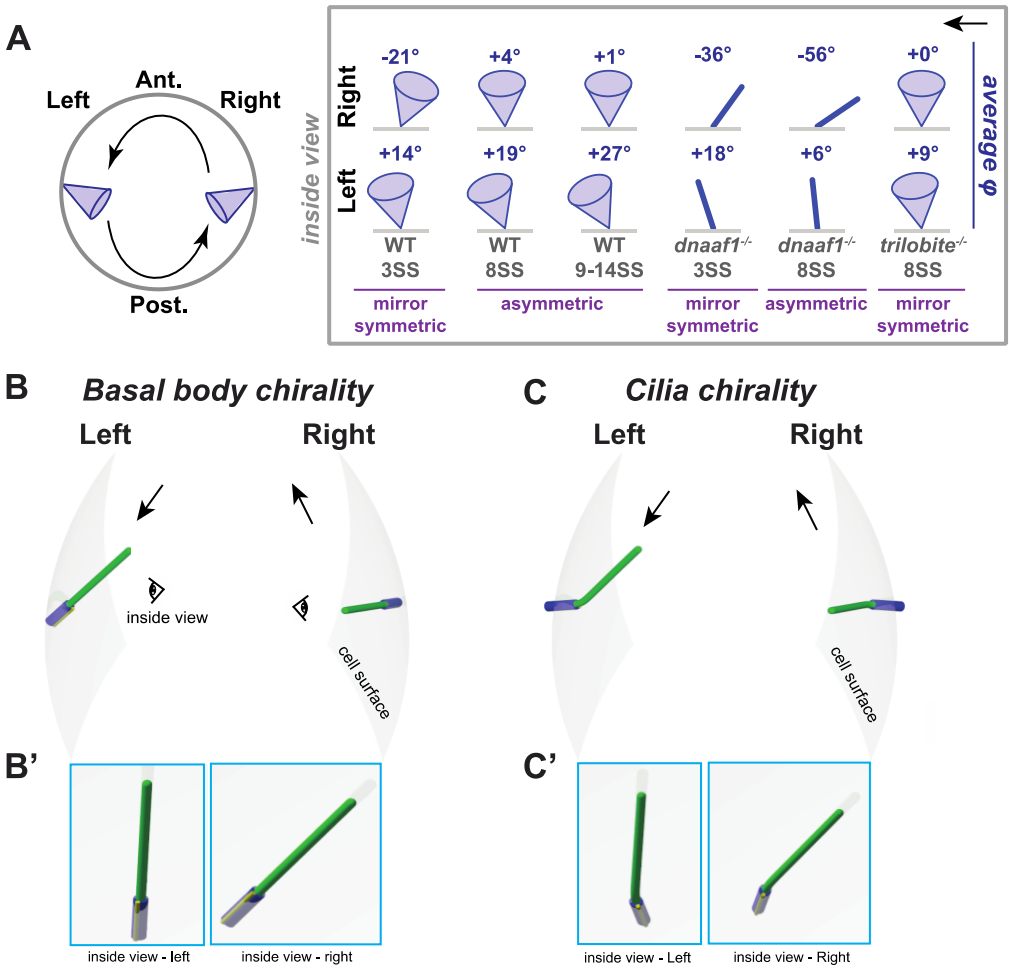

Figure 4

Figure 4: Schematic summary of the contributions of different pathways and the potential origins of chirality leading to asymmetric cilia orientation in the KV. (A) Left: Dorsal view of a mirror-symmetric KV showing a representative cilium on the left and on the right side. Right: schematic view of the average φ orientation over time in WT, *dnaaf1*$^{-/-}$ and *trilobite*$^{-/-}$ KV for cilia in the right (upper row) and in the left (lower row) KV hemispheres. KV is mirror-symmetric at 3SS both in WT and *dnaaf1*$^{-/-}$ embryos, evolving to an asymmetric orientation at 8SS. In contrast, *trilobite*$^{-/-}$ 8SS KVs do not show any evidence of asymmetry. **(B)** The orientation of basal bodies can be asymmetric between left and right. In this case, the chirality is of cellular origin. **(C)** Alternatively, the basal bodies can be arranged symmetrically, but the cilium itself has a chiral structure. The black arrows in A, B and C indicate the direction of the flow.

Materials and Methods

Zebrafish strains

The zebrafish (*Danio rerio*) lines used in this study were the following: *Tg*(*actb2:*Mmu.*Arl13b-GFP*) (Borovina et al., 2010), *Tg*(*dnaaf1*^{tm317b}*; actb2:*Mmu.*Arl13b-GFP*) (Sullivan-Brown et al., 2008), *Tg*(*trilobite*^{tc240a}*; actb2:*Mmu.*Arl13b-GFP*) (Heisenberg and Nusslein-Volhard, 1997), *Tg*(*spaw*^{s457}*; actb2:*Mmu.*Arl13b-GFP*) (Kalogirou et al., 2014), *Tg*(*cup*^{tc241}*; actb2:Arl13b-GFP*) (Schottenfeld et al., 2007). All zebrafish strains were maintained at the IGBMC fish facility under standard husbandry conditions (14h light/10h dark cycle). The Animal Experimentation Committee of the Institutional Review Board of IGBMC approved all animal experiments performed in this project.

Morpholino (MO) knockdown

MO designed to block the *rock2b* RNA splicing site (Wang et al., 2011) was obtained from *Gene Tools, LLC* and dissolved in water to a stock concentration of 3M. To deliver MO to all embryonic cells, 1-cell stage embryos were injected with 0.66ng of *rock2b*-MO (5'-GCACACACTCACTCACCAGCTGCAC-3'). Non-injected embryos were kept as controls.

Blebbistatin treatment

Embryos at bud-stage had the chorion removed and were treated with 35µM of Blebbistatin (SIGMA B0560/DMSO) at 32ºC in the dark. Non-treated embryos were kept in the dark at the same temperature and used to stage the development of the treated ones. When reaching the 3SS, treated embryos were washed carefully in 0.3% Danieau medium and kept at 32ºC until the desired developmental stage for live imaging (8SS). 1%-DMSO treated embryos were used to monitor potential drug-control effects.

2-photon excitation fluorescence microscopy (2PEF)

Live imaging experiments were performed as described in (Ferreira et al., 2017). To image deep enough into the zebrafish embryo and capture the entire Kupffer's vesicle (KV), each live embryo of the different conditions was imaged using 2PEF microscopy with a SP8 direct microscope (Leica Inc.) at 930nm wavelength (Chameleon Ultra laser, Coherent Inc.) using a low magnification high numerical aperture (NA) water immersion objective (Leica, 25x, 0.95 NA). We imaged the KV of embryos labeled with both *Arl13b*-eGFP and Bodipy TR at 3- and 8-somite stages (SSs): 100 x 100 x 50 µm^3 3D-stacks with 0.2 x 0.2 x 0.8 µm^3 voxel size and 2.4 µs pixel dwell time were typically acquired in order to maximize the scanning artifact allowing to properly reconstruct cilia orientation in 3D as described in (Supatto and Vermot, 2011). The fluorescence signal was collected using Hybrid internal detectors at 493-575 nm and 594-730 nm in order to discriminate the GFP signal labelling cilia from the signal labelling the KV cell surface. To uncover the orientation of the KV within the body axes, the midline was also imaged. We typically imaged a volume of 600 µm × 600 µm × 150 µm comprising the midline and the KV from top to bottom with a voxel size of 1.15 µm laterally and 5 µm axially. After imaging, embryos were released from the agarose mould and placed at

28.5° until 30hpf when the heart laterality was accessed. Further, when needed, embryos were genotyped by sequencing (detailed protocol described further in this section).

3D-Cilia Map: quantitative 3D cilia feature mapping

We used *3D-Cilia Map*, a quantitative imaging strategy to visualize and quantify the 3D biophysical features of all endogenous cilia in the KV in live zebrafish embryos, as described in (Ferreira et al., 2017).

Whole-mount *in situ* hybridization (WISH)

Whole-mount *in situ* hybridization was performed as described previously (Thisse and Thisse, 2008). Digoxigenin RNA probes were synthesized from DNA templates of *spaw* (Long, 2003) and *foxA3* (Monteiro et al., 2008). Embryos for *spaw* and *foxA3* WISH were fixed at 17SS and 53hpf respectively. After WISH, embryos were scored and kept in 20%-Glycerol/PBS at 4°C or genotyped.

Scoring of *spaw* expression, heart and gut looping

Embryos were collected after 15 min of contact between the mating pairs to guarantee homogeneity of the egg population. For heart and gut *situs* scoring experiments, embryos were raised at 28.5ºC in the dark in 0.3% Danieu medium supplemented with 0.003% (wt/v) 2-phenylthiourea to inhibit pigment formation and staged according to hours post-fertilization (hpf). For *spaw* expression patterns, embryos were raised at 25ºC in the dark in 0.3% Danieau medium and staged according to the number of somites. For both LR scoring experiments, whole clutches were used in order to perform robust population studies.

Spaw expression patterns in the lateral plate mesoderm (LPM) can be classified into four main categories: left, bilateral, right or absent (Sup. Figure 3A)(Long, 2003). The zebrafish heart looping was accessed at 48hpf when the heart is already beating. Due to its transparency, the heart loop can be visible under a regular binocular using brightfield illumination, and classified as: dextral, sinistral or absent. We performed WISH for *foxA3* at 53hpf in order to visualize the gut *situs* (Monteiro et al., 2008) in the same embryos we previously accessed the heart looping at 48hpf. Embryos were evaluated after WISH under a binocular using brightfield illumination and scored according to the curvature between the liver and the pancreas: left curvature (liver on the left, pancreas on the right), no curvature and right curvature (liver on the right and pancreas on the left). For the sake of simplicity, we merged the laterality information of both heart and gut and described it according to the clinical terminology: *situs solitus* (normal condition: heart with a dextral loop and left curvature of the gut), *situs inversus* (pathological condition characterized by a complete reversal of the organ laterality) and *heterotaxy* (pathological condition described by any combination of abnormal LR asymmetries that cannot be strictly classified as *situs solitus* or *situs inversus*) (Fliegauf et al., 2007; Ramsdell, 2005; Shapiro et al., 2014; Sutherland and Ware, 2009). After scoring, embryos with no visible mutant phenotype at 53hpf were genotyped individually (protocol described in this section and information provided in Table 3).

Quantifications and statistical analysis

To statistically test the mirror-symmetry in the KV, we used a permutation test (also called randomization test) (Hesterberg T, 2005). We compute the statistic $|\varphi_{avg_left} - \varphi_{avg_right\ mirror}|$, where φ_{avg_left} is the φ angle of the average resultant vector of left cilia and $\varphi_{avg_right\ mirror}$ is the φ angle of the resultant vector of right cilia after LR mirror symmetry. This statistic is based on the definition of chirality as we test if the left cilia orientation superimposes with the mirror image of right cilia. Left and right labels of cilia are then randomly permutated 300,000 times to construct the sampling distribution of possible $|\varphi_{avg_left} - \varphi_{avg_right\ mirror}|$ values. The one-sided p-value is finally estimated as the proportion of permutations resulting in values greater than or equal to the experimental one. We define the structure of the KV as chiral (or asymmetric) when the p-value is lower than 0.05 and the null hypothesis ($\varphi_{avg_left} = \varphi_{avg_right\ mirror}$) can be rejected. The same test is used to investigate θ mirror-symmetry. The p-values of the effective angular velocity vector ($\vec{\Omega}$) of all conditions against the WT were calculated using Welch's test on the dorsal component Ω_D.

Fluid dynamic simulations

We characterized the circulatory flow in the KV by calculating the effective angular velocity vector ($\vec{\Omega}$) as described in (Ferreira et al., 2017). We described each cilium in a KV as a chain of beads moving along a tilted cone with the orientation obtained from 3D-CiliaMap and calculated the flow using Green's function for the Stokes equation in the presence of a spherical no-slip boundary. The effective $\vec{\Omega}$ is defined as the angular velocity of a rotating rigid sphere with the same angular momentum as the time-averaged flow in the KV.

Genotyping strategies of adult fish and single embryos

Adult fish were anaesthetized with 80µg/mL Tricaine/MS-222 (Sigma, Cat. # A-5040) before cutting 1/3 of the caudal fin, and kept separated until the end of the genotyping experiments. Each piece of fin was kept in Lysis buffer at 55°C overnight with agitation. DNA extraction from fins was performed using sodium chloride, isopropanol and 70%-Ethanol. DNA samples were stored at -20ºC. PCR was performed in order to amplify the DNA fragments of interest for genotyping. All primers were designed with the program ApE (http://biologylabs.utah.edu/ jorgensen/wayned/ape/) and using the genomic sequences available on Ensemble (*Ensembl genome browser 84*) for *dnaaf1, spaw* and *cup* genes. The designed primers and mutation details are listed in Table 3.

DNA extracted from single embryos follows a distinct extraction procedure using sodium hydroxide (Meeker et al., 2007). Embryos from the *trilobite*^{tc240a} (Heisenberg and Nusslein-Volhard, 1997) mutant line were identifiable by phenotype at all the stages analyzed. *dnaaf1*^{tm317b} (Sullivan-Brown et al., 2008) *and cup*^{tc241} (Schottenfeld et al., 2007) mutant embryos were identifiable for heart and gut scoring analysis (48-53 hpf), and were genotyped only at earlier stages. *spaw*^{s457} (Kalogirou et al., 2014) mutant embryos were always genotyped by sequencing.

Supplementary figures

Supplemental Figure 1

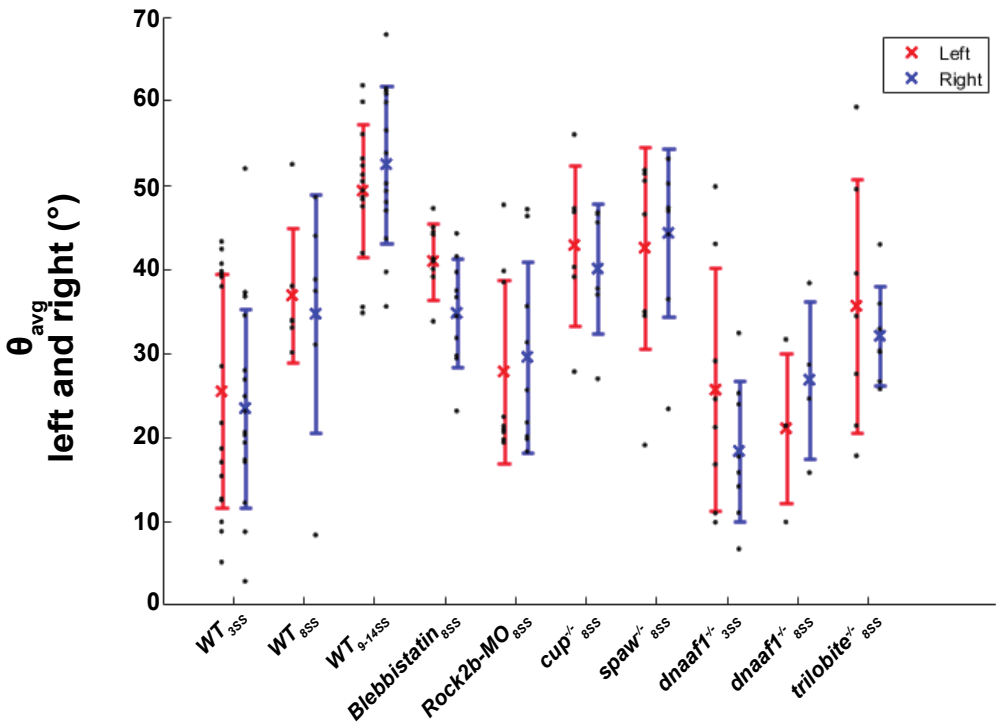

Sup. Figure 1: Distribution of θ angles on the right and on the left sides of the KV. Dot plot displaying the mean values of θ_{avg} on the left (in red) and on the right (in blue) sides of the KV for all conditions. Permutation tests show there are no signs of asymmetry relating to θ_{avg} in all conditions studied ($p > 0.05$).

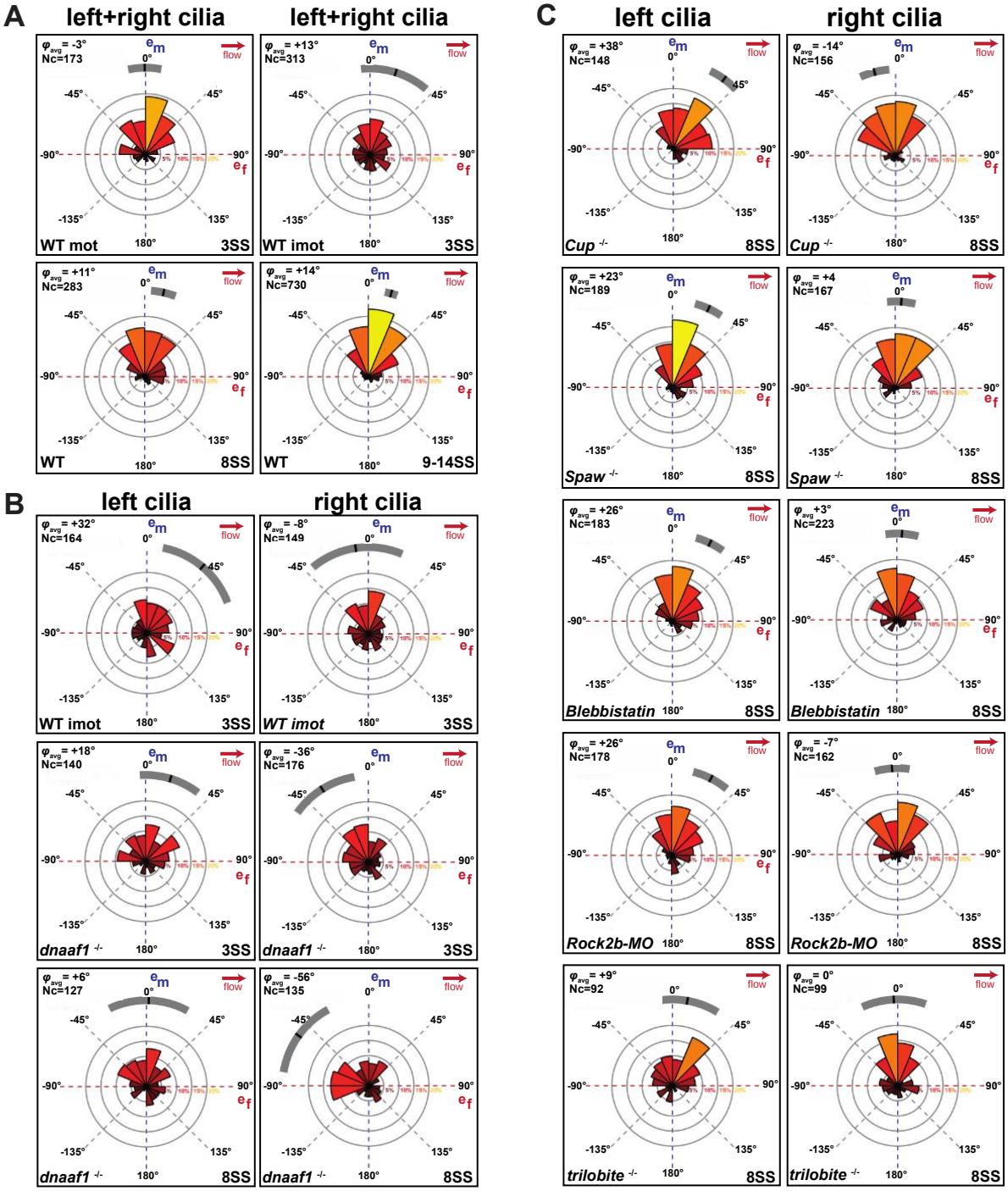

Supplemental Figure 2

Sup. Figure 2: Additional information about φ angle distributions displayed in rosette plots. Rosette plots showing the φ angle distribution and φ_{avg} values of cilia in both KV hemispheres (left+right cilia) for WT cilia at different stages **(A),** and left and right separately for the immotile cilia population in both WT and *dnaaf1*$^{-/-}$ **(B)** and for the *cup*$^{-/-}$, *spaw*$^{-/-}$, blebbistatin, *rock2b*-MO and *trilobite*$^{-/-}$ conditions **(C)**. All conditions presented asymmetric KVs at 8SS, with the exception of *trilobite*$^{-/-}$, which is mirror-symmetric like KVs analyzed at 3SS. Statistics provided in Table 1. Nc = number of cilia

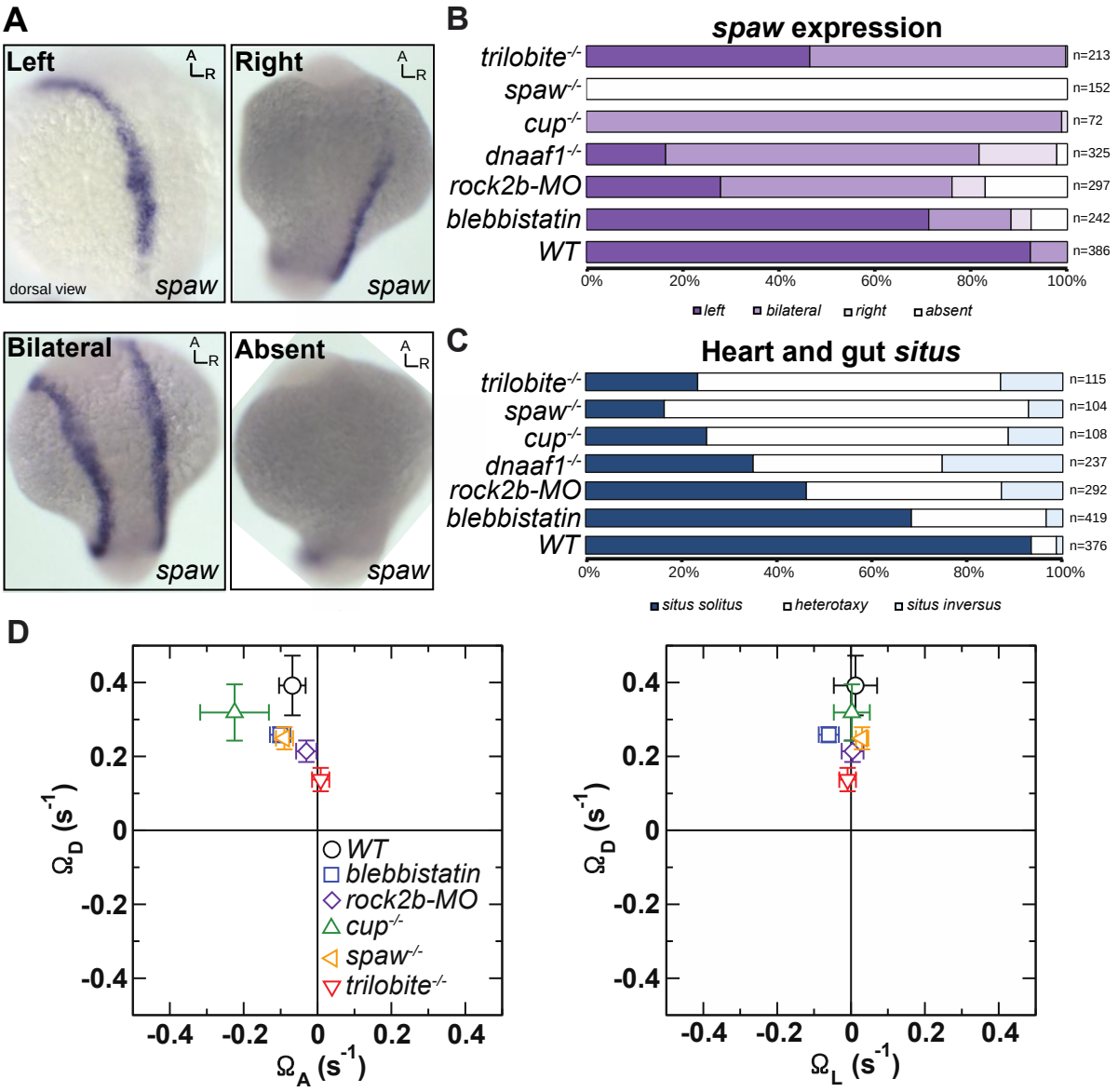

Supplemental Figure 3

Supplemental Figure 3: (A-C) Quantification of the spaw expression patterns in the LPM and heart and gut situs in all conditions studied. (A) *spaw* expression patterns in the LPM can be divided in left, bilateral, right or absent. **(B-C)** Percentages of *spaw* expression patterns in the LPM **(B)** and the *situs* phenotypes **(C)**. The number of embryos analyzed is displayed next to each bar. *Situs* phenotypes are classified according to the clinical terminology in *situs solitus*, *heterotaxy* and *situs inversus*. **(D)** Effective angular velocity ($\vec{\Omega}$) of the flow in the KV, determined computationally from cilia orientations and motility. The main graph shows the right view of the $\vec{\Omega}$ (dorsal vs. left anterior component), the insets show the anterior view (dorsal vs. left component). In contrast with the other conditions, *trilobite*$^{-/-}$ embryos have a significantly weaker flow (p=0.024) when compared to WT.

Table 1

Mirror-symmetry: $\varphi_{_Left} = -\varphi_{_right}$?	WT 3SS		WT	WT	*dnaaf1*$^{-/-}$	*dnaaf1*$^{-/-}$	Blebbistatin	*rock2b*-MO	*cup*$^{-/-}$	*spaw*$^{-/-}$	*trilobite*$^{-/-}$
	motile cilia	immotile cilia	8SS	9-14SS	3SS	8SS	8SS	8SS	8SS	8SS	8SS
p value	0.45	0.23	0.002	<0.001	0.23	0.008	<0.001	0.014	<0.001	<0.001	0.54

Table 2

	WT controls	blebbistatin	rock2b MO	*dnaaf1* $^{-/-}$	*cup* $^{/-}$	*spaw*$^{-/-}$	*trilobite* $^{-/-}$
	Mean ± SEM	Mean ± SEM	Mean ± SEM	Mean ± SEM	Mean ± SEM	Mean ± SEM	Mean ± SEM
left	92.3 ± 4.0%	71.2 ± 2.5%	27.9 ± 1.3%	16.5 ± 5.1%	0 ± 0%	0 ± 0%	46.5 ± 7.3%
bilateral	7.7 ± 4.0%	17.1 ± 4.8%	48.1 ± 4.0%	65.2 ± 11.1%	98.8 ± 1.2%	0 ± 0%	53.2 ± 6.9%
right	0 ± 0%	4.2 ± 1.1%	6.9 ± 0.5%	16.1 ± 5.1%	1.2 ± 1.2%	0 ± 0%	0%
absent	0 ± 0%	7.5 ± 1.3%	17.1 ± 5.9%	2.2 ± 1.3%	0 ± 0%	100 ± 0%	0.3 ± 0.4%
situs solitus	93.4 ± 0.6%	68.3 ± 4.3%	46.3 ± 3.0%	35.1 ± 1.4%	25.5 ± 4.6%	16.5 ± 0.6%	23.5 ± 0.2%
heterotaxy	5.3 ± 0.9%	28.3 ± 2.9%	40.9 ± 1.8%	39.6 ± 0.6%	63.5 ± 4.6%	76.3 ± 1.7%	63.5 ± 0.6%
situs inversus	1.3 ± 0.3%	3.5 ± 1.3%	12.9 ± 1.2%	25.3 ± 1.2%	11.5 ± 0.4%	7.2 ± 2.3%	13.0 ± 0.4%

Table 3

Line ID	References	Genotype			
		Primer sequences	PCR primers	Sequencing	Mutation
dnaaf1^{tm317b}; *actb2:*Mmu.*Arl13b-GFP*	Schottenfeld et al., 2007	PF1 : CCATTAGCCTGCACATTCAATC PR1 : ATCGCACTGCTCATCTGAAG	PF1/PR1	PF1	TGTT(A)GTGGGATAC
spaw^{s457}; *actb2:*Mmu.*Arl13b-GFP*	Sullivan-Brown et al., 2008	PF1seq : CTAGTTTGAGCGACTTGTCCA PR2 : CACCCGCTGGAAAGATCAAG PR1 : CACTGATGCGGTTGTGGGAC	PFseq1/PR2	PR1	CAGTGTG(T)TTATGAG
cup^{tc241}; *actb2:Arl13b-GFP*	Beis et al., 2005; Kalogirou et al., 2014	PF1 : GCTCTCTGATGTGCCTGACG PR1 : TCGATCCACACGCAATCAAC	PF1/PR1	PF1	CATTCGCAAT(A)GCA

Table 1: Statistical test of mirror-symmetry in the KV. The p-values result from a permutation test under the null hypothesis of a mirror-symmetric KV $\varphi_{avg_left} = -\varphi_{avg_right}$.

Table 2: Mean and SEM regarding the LR scoring (Supplemental Figure 3).

Table 3: Supplemental information concerning the genotyping strategies of the mutant lines used.

Movie 1: Cilia motility is impaired in the *dnaaf1*$^{-/-}$ embryos. The movie shows the 3D live imaging of two KVs from the *Tg*(*dnaaf1*^{tm317b}*; actb2:*Mmu.*Arl13b-GFP*)(Sullivan-Brown et al., 2008). Each embryo was soaked for 60 minutes in Bodipy TR (Molecular Probe) and imaged using 2PEF microscopy at 930 nm wavelength. A full z-stack of both KVs can be seen. On the left, a KV from a sibling *dnaaf1*$^{+/+}$ with motile cilia (fan cones) is shown. On the right, a KV from a *dnaaf1*$^{-/-}$ embryo, with 100% of immotile cilia (bright straight lines) is shown.

Acknowledgements

We thank C. Norden, M. Blum, and the Vermot lab for discussion and thoughtful comments on the manuscript, in particular R. Chow for her help with editing. We thank L. Klaeyle for great technical support. We also thank the Heisenberg lab for sharing the trilobite line. This work was supported by FRM (DEQ20140329553), the ANR (ANR-15-CE13-0015-01, ANR-12-ISV2-0001-01), the EMBO Young Investigator Program, the European Community, ERC CoG N°682938 Evalve and by the grant ANR-10-LABX-0030-INRT, a French State fund managed by the Agence Nationale de la Recherche under the frame program Investissements d'Avenir labeled ANR-10-IDEX-0002-02. R.R.F. was supported by the IGBMC International PhD program (LABEX). A.V. acknowledges support from the Slovenian Research Agency (grant P1-0099).

References

Afzelius, B.A. (1976). A human syndrome caused by immotile cilia. Science *193*, 317-319.

Blum, M., Schweickert, A., Vick, P., Wright, C.V., and Danilchik, M.V. (2014). Symmetry breakage in the vertebrate embryo: when does it happen and how does it work? Dev Biol *393*, 109-123.

Borovina, A., Superina, S., Voskas, D., and Ciruna, B. (2010). Vangl2 directs the posterior tilting and asymmetric localization of motile primary cilia. Nat Cell Biol *12*, 407-412.

Coutelis, J.B., Gonzalez-Morales, N., Geminard, C., and Noselli, S. (2014). Diversity and convergence in the mechanisms establishing L/R asymmetry in metazoa. EMBO Rep *15*, 926-937.

Dasgupta, A., and Amack, J.D. (2016). Cilia in vertebrate left-right patterning. Philos Trans R Soc Lond B Biol Sci *371*.

Davison, A., McDowell, G.S., Holden, J.M., Johnson, H.F., Koutsovoulos, G.D., Liu, M.M., Hulpiau, P., Van Roy, F., Wade, C.M., Banerjee, R.*, et al.* (2016). Formin Is Associated with Left-Right Asymmetry in the Pond Snail and the Frog. Curr Biol *26*, 654-660.

Essner, J.J., Amack, J.D., Nyholm, M.K., Harris, E.B., and Yost, H.J. (2005). Kupffer's vesicle is a ciliated organ of asymmetry in the zebrafish embryo that initiates left-right development of the brain, heart and gut. Development *132*, 1247-1260.

Faubel, R., Westendorf, C., Bodenschatz, E., and Eichele, G. (2016). Cilia-based flow network in the brain ventricles. Science *353*, 176-178.

Ferreira, R.R., Vilfan, A., Julicher, F., Supatto, W., and Vermot, J. (2017). Physical limits of flow sensing in the left-right organizer. Elife *6*.

Fliegauf, M., Benzing, T., and Omran, H. (2007). When cilia go bad: cilia defects and ciliopathies. Nat Rev Mol Cell Biol *8*, 880-893.

Francescatto, L., Rothschild, S.C., Myers, A.L., and Tombes, R.M. (2010). The activation of membrane targeted CaMK-II in the zebrafish Kupffer's vesicle is required for left-right asymmetry. Development *137*, 2753-2762.

Franco, C.A., Jones, M.L., Bernabeu, M.O., Geudens, I., Mathivet, T., Rosa, A., Lopes, F.M., Lima, A.P., Ragab, A., Collins, R.T.*, et al.* (2015). Dynamic endothelial cell rearrangements drive developmental vessel regression. PLoS Biol *13*, e1002125.

Goldstein, R.E. (2015). Green Algae as Model Organisms for Biological Fluid Dynamics. Annu Rev Fluid Mech *47*, 343-375.

Gomez-Lopez, S., Lerner, R.G., and Petritsch, C. (2014). Asymmetric cell division of stem and progenitor cells during homeostasis and cancer. Cell Mol Life Sci *71*, 575-597.

Grimes, D.T., Boswell, C.W., Morante, N.F., Henkelman, R.M., Burdine, R.D., and Ciruna, B. (2016). Zebrafish models of idiopathic scoliosis link cerebrospinal fluid flow defects to spine curvature. Science *352*, 1341-1344.

Gros, J., Feistel, K., Viebahn, C., Blum, M., and Tabin, C.J. (2009). Cell movements at Hensen's node establish left/right asymmetric gene expression in the chick. Science *324*, 941-944.

Guirao, B., Meunier, A., Mortaud, S., Aguilar, A., Corsi, J.M., Strehl, L., Hirota, Y., Desoeuvre, A., Boutin, C., Han, Y.G.*, et al.* (2010). Coupling between hydrodynamic forces and planar cell polarity orients mammalian motile cilia. Nat Cell Biol *12*, 341-350.

Hamada, H., and Tam, P.P. (2014). Mechanisms of left-right asymmetry and patterning: driver, mediator and responder. F1000Prime Rep *6*, 110.

Hashimoto, M., and Hamada, H. (2010). Translation of anterior-posterior polarity into left-right polarity in the mouse embryo. Curr Opin Genet Dev *20*, 433-437.

Heisenberg, C.P., and Nusslein-Volhard, C. (1997). The function of silberblick in the positioning of the eye anlage in the zebrafish embryo. Dev Biol *184*, 85-94.

Hesterberg T, M.D., Monaghan S, Clipson A & Epstein R. (2005). Bootstrap methods and permutation tests. Introduction to the Practice of Statistics 5th edn *16*, 1–70.

Hilfinger, A., and Julicher, F. (2008). The chirality of ciliary beats. Phys Biol *5*, 016003.

Hong, H., Kim, J., and Kim, J. (2015). Myosin heavy chain 10 (MYH10) is required for centriole migration during the biogenesis of primary cilia. Biochem Biophys Res Commun *461*, 180-185.

Hozumi, S., Maeda, R., Taniguchi, K., Kanai, M., Shirakabe, S., Sasamura, T., Speder, P., Noselli, S., Aigaki, T., Murakami, R.*, et al.* (2006). An unconventional myosin in Drosophila reverses the default handedness in visceral organs. Nature *440*, 798-802.

Jaffe, K.M., Grimes, D.T., Schottenfeld-Roames, J., Werner, M.E., Ku, T.S., Kim, S.K., Pelliccia, J.L., Morante, N.F., Mitchell, B.J., and Burdine, R.D. (2016). c21orf59/kurly Controls Both Cilia Motility and Polarization. Cell Rep *14*, 1841-1849.

Jessen, J.R., and Solnica-Krezel, L. (2004). Identification and developmental expression pattern of van gogh-like 1, a second zebrafish strabismus homologue. Gene Expr Patterns *4*, 339-344.

Kalogirou, S., Malissovas, N., Moro, E., Argenton, F., Stainier, D.Y., and Beis, D. (2014). Intracardiac flow dynamics regulate atrioventricular valve morphogenesis. Cardiovasc Res *104*, 49-60.

Kramer-Zucker, A.G., Olale, F., Haycraft, C.J., Yoder, B.K., Schier, A.F., and Drummond, I.A. (2005). Cilia-driven fluid flow in the zebrafish pronephros, brain and Kupffer's vesicle is required for normal organogenesis. Development *132*, 1907-1921.

Kuroda, R., Endo, B., Abe, M., and Shimizu, M. (2009). Chiral blastomere arrangement dictates zygotic left-right asymmetry pathway in snails. Nature *462*, 790-794.

Kwon, H.B., Wang, S., Helker, C.S., Rasouli, S.J., Maischein, H.M., Offermanns, S., Herzog, W., and Stainier, D.Y. (2016). In vivo modulation of endothelial polarization by Apelin receptor signalling. Nat Commun *7*, 11805.

Levin, M. (2005). Left-right asymmetry in embryonic development: a comprehensive review. Mech Dev *122*, 3-25.

Loges, N.T., Olbrich, H., Becker-Heck, A., Haffner, K., Heer, A., Reinhard, C., Schmidts, M., Kispert, A., Zariwala, M.A., Leigh, M.W.*, et al.* (2009). Deletions and point mutations of LRRC50 cause primary ciliary dyskinesia due to dynein arm defects. Am J Hum Genet *85*, 883-889.

Long, S. (2003). The zebrafish nodal-related gene southpaw is required for visceral and diencephalic left-right asymmetry. Development *130*, 2303-2316.

Marshall, W.F. (2012). Centriole asymmetry determines algal cell geometry. Curr Opin Plant Biol *15*, 632-637.

Marshall, W.F., and Kintner, C. (2008). Cilia orientation and the fluid mechanics of development. Curr Opin Cell Biol *20*, 48-52.

Meeker, N.D., Hutchinson, S.A., Ho, L., and Trede, N.S. (2007). Method for isolation of PCR-ready genomic DNA from zebrafish tissues. Biotechniques *43*, 610, 612, 614.

Mitchell, D.R. (2003). Orientation of the central pair complex during flagellar bend formation in Chlamydomonas. Cell Motil Cytoskeleton *56*, 120-129.

Mitchison, H.M., and Valente, E.M. (2017). Motile and non-motile cilia in human pathology: from function to phenotypes. J Pathol *241*, 294-309.

Monteiro, R., van Dinther, M., Bakkers, J., Wilkinson, R., Patient, R., ten Dijke, P., and Mummery, C. (2008). Two novel type II receptors mediate BMP signalling and are required to establish left-right asymmetry in zebrafish. Dev Biol *315*, 55-71.

Morrow, S.M., Bissette, A.J., and Fletcher, S.P. (2017). Transmission of chirality through space and across length scales. Nat Nanotechnol *12*, 410-419.

Naganathan, S.R., Furthauer, S., Nishikawa, M., Julicher, F., and Grill, S.W. (2014). Active torque generation by the actomyosin cell cortex drives left-right symmetry breaking. Elife *3*, e04165.

Noel, E.S., Verhoeven, M., Lagendijk, A.K., Tessadori, F., Smith, K., Choorapoikayil, S., den Hertog, J., and Bakkers, J. (2013). A Nodal-independent and tissue-intrinsic mechanism controls heart-looping chirality. Nat Commun *4*, 2754.

Okada, Y., Takeda, S., Tanaka, Y., Izpisua Belmonte, J.C., and Hirokawa, N. (2005). Mechanism of nodal flow: a conserved symmetry breaking event in left-right axis determination. Cell *121*, 633-644.

Pearson, C.G. (2014). Choosing sides--asymmetric centriole and basal body assembly. J Cell Sci *127*, 2803-2810.

Pitaval, A., Tseng, Q., Bornens, M., and Thery, M. (2010). Cell shape and contractility regulate ciliogenesis in cell cycle-arrested cells. J Cell Biol *191*, 303-312.

Qiu, D., Cheng, S.M., Wozniak, L., McSweeney, M., Perrone, E., and Levin, M. (2005). Localization and loss-of-function implicates ciliary proteins in early, cytoplasmic roles in left-right asymmetry. Dev Dyn *234*, 176-189.

Ramsdell, A.F. (2005). Left-right asymmetry and congenital cardiac defects: getting to the heart of the matter in vertebrate left-right axis determination. Dev Biol *288*, 1-20.

Sarmah, B., Latimer, A.J., Appel, B., and Wente, S.R. (2005). Inositol polyphosphates regulate zebrafish left-right asymmetry. Dev Cell *9*, 133-145.

Satir, P. (2016). Chirality of the cytoskeleton in the origins of cellular asymmetry. Philos Trans R Soc Lond B Biol Sci *371*.

Sato, K., Hiraiwa, T., Maekawa, E., Isomura, A., Shibata, T., and Kuranaga, E. (2015). Left-right asymmetric cell intercalation drives directional collective cell movement in epithelial morphogenesis. Nat Commun *6*, 10074.

Schottenfeld, J., Sullivan-Brown, J., and Burdine, R.D. (2007). Zebrafish curly up encodes a Pkd2 ortholog that restricts left-side-specific expression of southpaw. Development *134*, 1605-1615.

Shapiro, A.J., Davis, S.D., Ferkol, T., Dell, S.D., Rosenfeld, M., Olivier, K.N., Sagel, S.D., Milla, C., Zariwala, M.A., Wolf, W.*, et al.* (2014). Laterality defects other than situs inversus totalis in primary ciliary dyskinesia: insights into situs ambiguus and heterotaxy. Chest *146*, 1176-1186.

Shibazaki, Y., Shimizu, M., and Kuroda, R. (2004). Body handedness is directed by genetically determined cytoskeletal dynamics in the early embryo. Curr Biol *14*, 1462-1467.

Shinohara, K., and Hamada, H. (2017). Cilia in Left-Right Symmetry Breaking. Cold Spring Harb Perspect Biol *9*.

Song, H., Hu, J., Chen, W., Elliott, G., Andre, P., Gao, B., and Yang, Y. (2010). Planar cell polarity breaks bilateral symmetry by controlling ciliary positioning. Nature *466*, 378-382.

Speder, P., Adam, G., and Noselli, S. (2006). Type ID unconventional myosin controls left-right asymmetry in Drosophila. Nature *440*, 803-807.

Sullivan-Brown, J., Schottenfeld, J., Okabe, N., Hostetter, C.L., Serluca, F.C., Thiberge, S.Y., and Burdine, R.D. (2008). Zebrafish mutations affecting cilia motility share similar cystic phenotypes and suggest a mechanism of cyst formation that differs from pkd2 morphants. Dev Biol *314*, 261-275.

Sutherland, M.J., and Ware, S.M. (2009). Disorders of left-right asymmetry: heterotaxy and situs inversus. Am J Med Genet C Semin Med Genet *151C*, 307-317.

Taber, L.A. (2006). Biophysical mechanisms of cardiac looping. Int J Dev Biol *50*, 323-332.

Tabin, C.J., and Vogan, K.J. (2003). A two-cilia model for vertebrate left-right axis specification. Genes Dev *17*, 1-6.

Tamm, S.L., Sonneborn, T.M., and Dippell, R.V. (1975). The role of cortical orientation in the control of the direction of ciliary beat in Paramecium. J Cell Biol *64*, 98-112.

Tee, Y.H., Shemesh, T., Thiagarajan, V., Hariadi, R.F., Anderson, K.L., Page, C., Volkmann, N., Hanein, D., Sivaramakrishnan, S., Kozlov, M.M.*, et al.* (2015). Cellular chirality arising from the self-organization of the actin cytoskeleton. Nat Cell Biol *17*, 445-457.

Thisse, C., and Thisse, B. (2008). High-resolution in situ hybridization to whole-mount zebrafish embryos. Nat Protoc *3*, 59-69.

Wagnière, G.H. (2007). On Chirality and the Universal Asymmetry: Reflections on Image and Mirror Image. Weinheim, Germany: Wiley-VCH.

Wallingford, J.B. (2012). Planar cell polarity and the developmental control of cell behavior in vertebrate embryos. Annu Rev Cell Dev Biol *28*, 627-653.

Wan, L.Q., Ronaldson, K., Park, M., Taylor, G., Zhang, Y., Gimble, J.M., and Vunjak-Novakovic, G. (2011). Micropatterned mammalian cells exhibit phenotype-specific left-right asymmetry. Proc Natl Acad Sci U S A *108*, 12295-12300.

Wang, G., Cadwallader, A.B., Jang, D.S., Tsang, M., Yost, H.J., and Amack, J.D. (2011). The Rho kinase Rock2b establishes anteroposterior asymmetry of the ciliated Kupffer's vesicle in zebrafish. Development *138*, 45-54.

Wang, G., Manning, M.L., and Amack, J.D. (2012). Regional cell shape changes control form and function of Kupffer's vesicle in the zebrafish embryo. Dev Biol *370*, 52-62.

Xu, J., Van Keymeulen, A., Wakida, N.M., Carlton, P., Berns, M.W., and Bourne, H.R. (2007). Polarity reveals intrinsic cell chirality. Proc Natl Acad Sci U S A *104*, 9296-9300.

Yuan, S., Zhao, L., Brueckner, M., and Sun, Z. (2015). Intraciliary calcium oscillations initiate vertebrate left-right asymmetry. Curr Biol *25*, 556-567.